ACADEMIC PRESS

Available online at www.sciencedirect.com
SCIENCE DIRECT®

Journal of Colloid and Interface Science 264 (2003) 20–29

JOURNAL OF Colloid and Interface Science

www.elsevier.com/locate/jcis

Low Peclet mass transport in assemblages of spherical particles for two different adsorption mechanisms

F.A. Coutelieris,* M.E. Kainourgiakis, and A.K. Stubos

National Center for Scientific Research "Demokritos," 15310 Aghia Paraskevi Attikis, Greece

Received 3 December 2002; accepted 20 March 2003

Abstract

The problem of flow and mass transport within an assemblage of spherical solid absorbers is investigated. We present and compare results from the numerical solution of the convection–diffusion equation in the sphere-in-cell geometry and in stochastically constructed 3-D spherical particle assemblages. In the first case, we make use of an analytical solution of the creeping flow field in the sphere-in-cell model while in the second we employ a full numerical solution of the flow field in the realistic geometry of sphere assemblages. Low to moderate Peclet numbers ($Pe < 10^2$) are considered where the validity of the sphere-in-cell model is uncertain. On the other hand, the selected porosities range from values close to unity, where the sphere-in-cell approximation is expected to hold, to intermediate values, where its applicability becomes again uncertain. In all cases, instantaneous and Langmuir adsorption is studied. It is found that the simplified sphere-in-cell approach performs adequately provided that proper account of the actual porous media properties (porosity and internal surface area) is taken. A simple match of porosity is not sufficient for a reliable estimation of adsorption efficiencies.
© 2003 Elsevier Inc. All rights reserved.

Keywords: Granular media; Peclet number; Adsorption; Flow; Mass transfer

1. Introduction

Numerous industrial and technological applications involving fluid flow and mass transport processes within multiparticle assemblages have attracted scientific interest in recent decades, mainly focusing on industrial physicochemical processes (sedimentation, catalysis, etc.), alternative energy sources (fuel cells, etc.), and separation techniques (chromatography, filters, etc.). Although arrays of regularly spatially distributed spheres represent an idealization of real granular media, they have been widely studied from both the fluid dynamics and mass transport points of view [1,2]. On the other hand, due to the complexity of their geometry, random particle distributions have been the subject of rather limited investigations until about 20 years ago (see [3,4]). Since then, fast advances in computational capabilities contributed to reviving the interest in this topic with emphasis placed on hydrodynamic aspects [5–7].

Of practical importance is the case of low Reynolds number flow where analytical solutions can be obtained for the flow field and the mass diffusion and/or adsorption process in a simplified geometry (sphere-in-cell model). The fundamental approach of Happel [8] and the equivalent but independently presented model of Kuwabara [9] constitute initial attempts in the direction of analytical derivation of the velocity field under creeping flow conditions in the sphere-in-cell geometry (see Fig. 1a) while the subsequent works of Neale and co-workers [10–12] extended further these pioneering studies. Considerable effort has also been invested in the numerical study of the creeping (Stokes) flow in the sphere-in-cell representation of the actual geometry of particle assemblages [13–15]. In addition, numerical solutions of the Stokes equations in realistic reconstructions of porous media and spherical assemblies have been presented in various contexts, usually with reference to material transport properties calculations [16,17].

When low concentration of the solute is assumed, the above approaches for the calculation of the velocity field can be very useful for the study of mass transfer from the fluid to the solid mass and vice versa. The first treatment of the problem is due to Levich [18], where a single isolated and instantaneously adsorbing solid sphere within an unbounded moving fluid is considered and an analytical solution for

* Corresponding author.
E-mail address: frank@ipta.demokritos.gr (F.A. Coutelieris).

0021-9797/03/$ – see front matter © 2003 Elsevier Inc. All rights reserved.
doi:10.1016/S0021-9797(03)00309-6

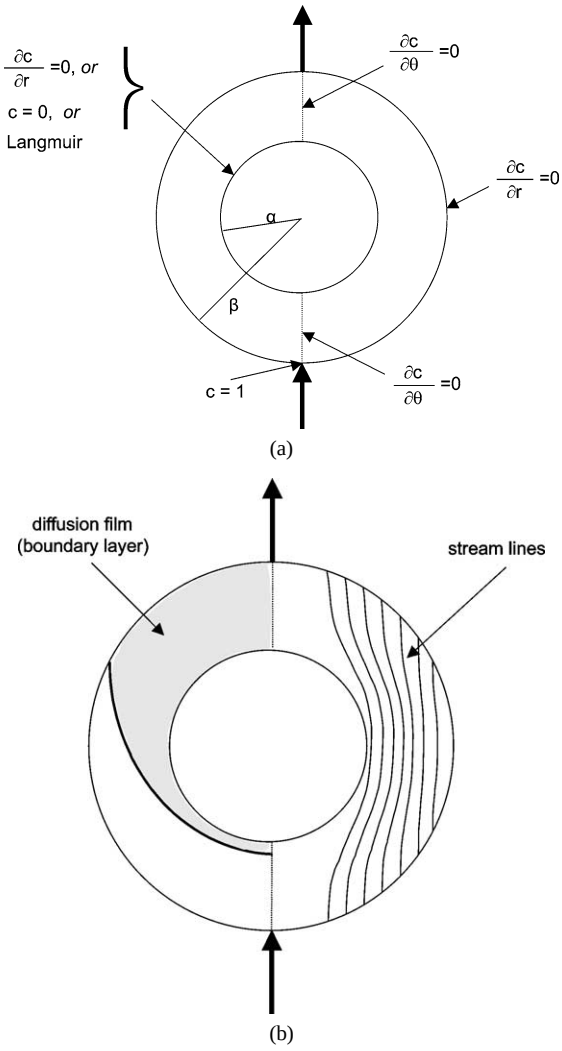

Fig. 1. The sphere-in-cell model (a) and the flow field and concentration boundary layer therein (b). Bold arrows indicate the fluid flow direction.

creeping flow conditions and high Peclet values ($Pe \gg 1$) is presented. The approach of Levich yields a simple analytical expression for the overall Sherwood number, *Sh*, of the form $Sh = 0.997Pe^{1/3}$. Note that *Pe* denotes the Peclet number, defined as $Pe = UL/D$, which expresses the ratio of the convective over diffusive forces in the flow regime. On the other hand, the overall Sherwood number, defined as $Sh = k_0 L/D$, expresses the ratio of the overall mass transport rate over the diffusive rate. Here, k_0 stands for the mass transfer coefficient, L is the characteristic length, U is the bulk fluid velocity, and D is the diffusion coefficient.

Based on a methodology similar to that of Levich, Pfeffer and Happel [19,20] and Sirkar [21] used Happel's model [8] to solve the problem of mass transfer to a sphere in a swarm for the high Peclet number case and obtained expressions of the form $Sh = f(\varepsilon)Pe^{1/3}$, where $f(\varepsilon)$ is a simple analytic function of the porosity, ε. In parallel, Tardos et al. [22] proposed correlations of the form $Sh = 0.997g(\varepsilon)Pe^{1/3}$, using Happel [8], Kuwabara [9], and Neal and co-workers [10–12] models, where $g(\varepsilon)$ is a model-dependent function of the porosity. The review paper by Quintard and Whitaker [23] summarizes the analytical, numerical, and experimental work performed on correlating *Sh* and *Pe* in sphere-in-cell types of geometry, sphere packs, and other granular media. It should also be mentioned that a series of publications [24–26] have studied numerically situations where dissolution or deposition processes occur in the pore space with simultaneous change of the porosity of the medium. Uniform deposition is found at relatively low Damkohler numbers; however, it is clear that our work and all the references cited examine interfacial processes not affecting the pore size.

In particular, the case of low Peclet values is more complicated as far as the mass transport problem is concerned since all the terms of the convection–diffusion equation that describes it "survive" and, thus, analytical solutions can be obtained only for special cases while numerical treatment is in general necessary. Some analytical expressions in pure diffusional environments ($Pe = 0$) have been presented in recent decades [27–29]. More recently, Romero [30] used an asymptotic expansion scheme to obtain an analytical solution for the low *Pe* flow and mass transfer past a single sphere while Han et al. [31] used similarity transformation techniques to analytically solve the problem of forced convective heat and mass transfer around a spherical particle having fluid surface properties. On the other hand, numerical solutions for mass transport problems under instantaneous adsorption have been rarely presented because in the majority of applications adsorption does not occur instantaneously [32]. Recently, a general expression for the overall Sherwood number as a function of the porosity has been proposed by Burganos et al. [33] for a wide range of particle shapes and Peclet values. This is based on analytical flow field treatment (particle-in-cell) and both analytical and numerical handling of the convection–diffusion equation in the particle-in-cell geometry for high and low Peclet numbers, respectively. It must be pointed out here that, at high *Pe*, Levich's approach [18] in combination with the analytical flow field of the sphere-in-cell geometry describes with sufficient accuracy the problem under consideration as both the flow and mass transfer aspects can be treated fully analytically (certain diffusive terms can be safely simplified) [18,22,33].

In almost all of the above-mentioned works, it has been assumed that the solid grains adsorb instantaneously the solute. Note that in these publications as well as in the rest of this study by instantaneous adsorption it is meant an "irreversible" adsorption process where the adsorbing surface operates as a sink of the diffusing substance. As instantaneous adsorption is not a frequent physicochemical phenomenon, several attempts toward modeling more realistic adsorption mechanisms on solid surfaces have been made. In this respect, Wen and Wei [34] analyzed, under no-flow conditions, the kinetics of simultaneous noncatalytic solid–gas reaction systems and produced a simple mathematical description for the adsorption rate. Further advancements in

the same direction were made by Lu et al. [35] who proposed a simple generalized gas–solid reaction model. More complicated models for the gas adsorption on solid surfaces by using first-order heterogeneous reactions were proposed by Wanker et al. [36], who modeled a single one-channel catalytic reactor, by Coutelieris [37], who presented a realistic adsorption–first-order reaction–desorption mechanism for solid spheroidal absorbers, and by Mat and Kaplan [38], who proposed a complicated description of the reaction rate for the representation of the metal hydride formation in a hydrogen storage tank. In parallel, Rosen [39] and Weber and Chakravorti [40] used Langmuir type of isotherms to describe the diffusion regime within a generalized fixed-bed absorber while Shams [41] employed a somehow more complicated sorption/desorption scheme to obtain analytical solution of the transient equations for the sorption/desorption in a fixed bed packed with thin-film-coated monodisperse spherical particles.

In the present work, we focus on relatively low *Pe* numbers and attempt a comparison between the semi-analytical approaches used in the large majority of the studies so far and the full solution of the flow and mass transfer problem in sphere assemblies. In particular, we present and compare the following:

(i) results based on the analytical solution of the flow field in the sphere-in-cell geometry and the subsequent numerical solution of the mass transport problem in the same geometry and for different adsorption modes;
(ii) results based on the numerical solution of the creeping flow field in stochastically constructed 3-D sphere assemblages and the subsequent numerical solution of the convection–diffusion problem in this realistic geometry under the same adsorption modes as in the above step.

The range of *Pe* considered in our work includes relatively low values where the validity of the sphere-in-cell model in representing adequately the geometry of the spherical particle assemblage is questionable. It is already mentioned above that at high *Pe* the overall problem is amenable to analytical treatment with sufficient accuracy in the simplified geometry of the sphere-in-cell model as the flow field therein can be taken as an approximation of the real one and diffusive terms can be significantly simplified. On the other hand, the selected porosities vary from very large values (close to unity) where the sphere-in-cell approximation is expected to hold to intermediate values where its applicability becomes again uncertain. Three different cases for the adsorption upon the solid surface are considered: (a) noadsorption, (b) instantaneous adsorption, and (c) adsorption according to Langmuir isotherm. The adsorption efficiency is calculated in all cases and appropriate comparisons are made. The paper is organized as follows: The sphere-in-cell model geometry is presented first along with the analytical solution for the respective flow field and the numerical formulation of the mass transport therein. The same problem is then examined in the realistic domain of a stochastically constructed sphere assembly. The results are discussed and compared in terms of the adsorption efficiency as a function of the porosity and the Peclet number. Finally, the main conclusions of the study are summarized.

2. Sphere-in-cell model

The sphere-in-cell geometry has been repeatedly used as a simple model for the representation of the actual complicated geometry of the pore space in spherical particle assemblages and the approximation of the flow field therein. Consider a solid sphere of radius α, which is surrounded by another concentric spherical liquid envelope of radius β, whose thickness is adjusted so that the porosity of the medium is equal to that of the model geometry (see Fig. 1a). The approaching fluid is a dilute solution of substance A, which is moving toward the solid adsorbing surface. The governing equation for the steady state mass transport in the fluid phase within the model can be written in spherical coordinates as

$$u_r\frac{\partial c_A}{\partial r}+\frac{u_\theta}{r}\frac{\partial c_A}{\partial \theta} = D\left(\frac{\partial^2 c_A}{\partial r^2}+\frac{2}{r}\frac{\partial c_A}{\partial r}+\frac{1}{r^2}\frac{\partial^2 c_A}{\partial \theta^2}+\frac{\cot\theta}{r^2}\frac{\partial c_A}{\partial \theta}\right), \tag{1}$$

where c_A is the concentration of substance A in the fluid phase, u_r and u_θ are the r- and θ-velocity components, and D is the diffusion coefficient of substance A in the solute. The velocity components are given as [9]

$$u_r=-2\left[\frac{F_1}{r^3}+\frac{F_2}{r}+F_3+F_4r^2\right]\cos\theta, \tag{2a}$$

$$u_\theta=-\left[\frac{F_1}{r^3}-\frac{F_2}{r}-2F_3-4F_4r^2\right]\sin\theta, \tag{2b}$$

where

$$F_1=-\frac{U}{4F_5}\left(1-2\frac{a^3}{b^3}\right), \tag{2c}$$

$$F_2=-\frac{3U}{4F_5}, \tag{2d}$$

$$F_3=-\frac{U}{2F_5}\left(1+\frac{a^3}{2b^3}\right), \tag{2e}$$

$$F_4=-\frac{3U}{20F_5}\left(\frac{b^3}{a^3}\right), \tag{2f}$$

$$F_5=\left(1-\frac{a}{b}\right)^3\left(1+\frac{6b}{5a}+\frac{3b^2}{5a^2}+\frac{b^3}{5a^3}\right), \tag{2g}$$

and U is the approaching fluid (bulk) velocity far from the solid surface. A typical representation of the flow field described by Eqs. (2a) and (2b) is included in Fig. 1b in the form of streamlines.

The axial symmetry of the mass transfer problem is expressed by the following boundary conditions:

$$\left.\frac{\partial c_A}{\partial \theta}\right]_{\theta=\pi} = 0, \quad \alpha < r \leqslant \beta, \tag{3a}$$

$$\left.\frac{\partial c_A}{\partial \theta}\right]_{\theta=0} = 0, \quad \alpha < r \leqslant \beta. \tag{3b}$$

To ensure the continuity of concentration for any Peclet number, Coutelieris et al. [42] proposed the following boundary condition at the outer boundary of the cell:

$$c_A(r=\beta, \theta=\pi) = 1, \tag{4a}$$

$$\left.\frac{\partial c_A}{\partial r}\right]_{r=\beta} = 0, \quad 0 \leqslant \theta < \pi. \tag{4b}$$

For high Peclet values, this boundary condition is completely equivalent to the well-known Levich approach for unbounded fluids, given elsewhere as $c_A = 1$ for $r \to \infty$ or $r = \beta$ [18,22]. Figure 1b provides an idea of the extent of the concentration boundary layer surrounding the solid surface.

Three different cases for the adsorption of the solute upon the solid surface are considered. The first case corresponds to neutral solid surface, i.e., to the complete absence of adsorption. This can be described by the following boundary condition upon the solid surface:

$$\left.\frac{\partial c_A}{\partial r}\right]_{r=\alpha} = 0, \quad 0 \leqslant \theta \leqslant \pi. \tag{5}$$

The second case corresponds to instantaneous adsorption upon the solid surface and can be expressed as

$$c_A(r=\alpha, \theta) = 0, \quad 0 \leqslant \theta \leqslant \pi. \tag{6}$$

Finally, the third case refers to adsorption following a Langmuir type of isotherm and can be formulated as

$$D\left.\frac{\partial c_A}{\partial r}\right]_{r=\alpha} = \frac{k}{K} c_s, \quad 0 \leqslant \theta \leqslant \pi, \tag{7}$$

where K is defined by the Langmuir isotherm

$$\Theta_{eq} = \frac{K c_b}{1 + K c_b}, \tag{8}$$

and k is a reaction rate defined from the relation

$$R(c_s) = k c_b (c_{mx} - c_s), \tag{9}$$

where $R(c_s)$ is the overall adsorption rate given as a function of the surface concentration c_s, c_b is the concentration of the diluted mass in the neighborhood of the solid surface, c_{mx} is the maximum concentration attained when the surface is completely covered by substance A, and Θ_{eq} is the ratio of the covered to the total surface, defined as

$$\Theta_{eq} = \frac{c_s}{c_{mx}}. \tag{10}$$

The adsorption efficiency of a grain in cell is defined by the ratio of the rate that the solute is adsorbed divided by the rate of the upstream influx. In general, it can be written as

$$\lambda_0 = \frac{\iint_{S_{sphere}} [-N_{A_r}]_{r=a}\, dS_{sphere}}{u_\infty c_{A,\infty} 4\pi\beta^2}, \tag{11}$$

where $[-N_{A_r}]_{r=a}$ is the r-component of the molar flux on the collector surface. It can be easily shown that

$$\lambda_0 = \frac{a^2}{4\pi\beta^2} \int_0^\pi \sin\theta \left(\frac{\partial(c_A/c_{A,\infty})}{\partial(r/\alpha)}\right)_{r=\alpha} d\theta. \tag{12}$$

Obviously, the boundary value problem of differential equation (1) with boundary conditions given by Eqs. (3a) and (3b), Eqs. (4a) and (4b), and Eq. (5) results in a uniform concentration profile $c_A(r, \theta) = 1$ for any r- and θ-values. To solve the instantaneous or Langmuir adsorption problems described by Eqs. (1), (3a) and (3b), (4a) and (4b), and (6) or (7), a nonuniform finite-difference scheme has been employed. For these cases, the value of λ_0 can be calculated once the r-component of the concentration gradient upon the surface is known by using a modified Newton–Cotes numerical method with adjustable step for the integration. The presently adopted numerical scheme has been validated against the adsorption efficiency values computed by Coutelieris et al. [42] for spheroidal geometry. Indeed, excellent agreement is obtained with the results of [42] when the axis ratio of either the prolate or the oblate spheroidal absorber is set to unity.

3. Solution of the flow and mass transfer problem in spherical particle assemblages

To define a realistic domain for the solution of the flow and mass transfer problem, a porous medium is constructed in the form of a spherical particle assemblage. Specifically, the representation of the biphasic domains under consideration is achieved by the random deposition of spheres of a given radius in a box of specified length. The structure is digitized and the phase function (equal to zero for solid and unity for the pore space) is determined to obtain the specified porosity (see Fig. 2a for a sample medium of $\varepsilon = 0.7243$). The size of the digitized domains is $102 \times 102 \times 102$ and the length of the simulation box is ten times the sphere radius.

The creeping flow of a Newtonian incompressible fluid within the pore space of the medium is described by the Stokes equation coupled with the continuity equation,

$$\mu \nabla^2 \mathbf{v} = \nabla p, \tag{13a}$$

$$\nabla \cdot \mathbf{v} = 0, \tag{13b}$$

where μ is the fluid viscosity, $\mathbf{v}$ is the local (interstitial) fluid velocity, and p is the local pressure. The boundary conditions for $\mathbf{v}$ are spatial periodicity and no-slip at the surface of the solid unit elements. In this work, the numerical solution of Eqs. (13a) and (13b) is achieved with the use

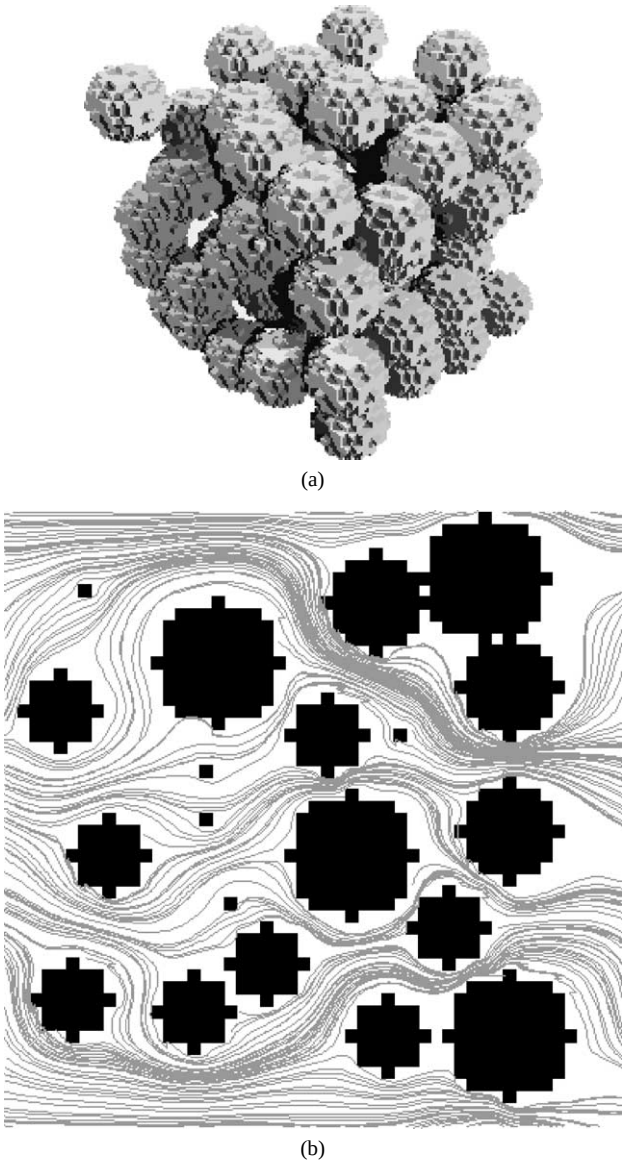

(a)

(b)

Fig. 2. Stochastically constructed 3-D sphere assemblage for $\varepsilon = 0.7243$ (a) and streamlines in a representative 2-D cut (b).

of a finite-difference scheme in conjunction with the artificial compressibility relaxation algorithm (see [43–45]). The pore space is discretized through a marker-and-cell (MAC) mesh with the pressure defined at the center of the cell and the velocity components defined along the corresponding face boundaries. The resulting linear system of equations is solved by the successive over-relaxation method. The present numerical scheme for the determination of the velocity field has been used and validated by the present authors in [45] where the calculated permeability of a random sphere pack was found in excellent agreement with that predicted by the Blake–Kozeny relation [46]. For visualization purposes, the flow field (streamlines) calculated in a representative 2-D cut of the sphere assembly is shown in Fig. 2b.

The time-dependent mass transport of a passive solute in the medium is described by the convection–diffusion equation (to be solved using the velocity field computed from Eqs. (13a) and (13b)):

$$\frac{\partial c_A}{\partial t} + \nabla \cdot (\mathbf{v} c_A) = D \nabla^2 c_A. \tag{14}$$

The three different adsorption modes employed above in the sphere-in-cell model, i.e., Eqs. (5)–(7), are also considered at the present fluid–solid interfaces. The equations describing the boundary value problem are discretized using finite differences with an upwind numerical scheme where the type (forward or backward) of the discretization of the local first derivatives in any direction is chosen depending on the actual direction of the velocity component in every location in the domain. This approach is known to ensure convergence up to moderate Peclet values. The resulting linear systems of equations are solved using the SOR technique. Finally, the adsorption efficiency is determined as

$$\lambda_0 = \frac{\iint_{S_{\text{outlet}}} c_A \mathbf{u} \cdot \mathbf{n}\, dS}{\iint_{S_{\text{inlet}}} c_A \mathbf{u} \cdot \mathbf{n}\, dS}. \tag{15}$$

The validity of the solution scheme for the mass transport problem of Eq. (14) is checked in the limiting case of a periodic array of spheres with radius R, which is fed at $x = 0$ by a concentration pulse. The concentration profile with time at the outlet ($x = L = 51R/8$) is then expressed as [47]

$$c(t) = \frac{1}{\sqrt{4\pi D^* t}} \exp\left[\frac{-(L-ut)^2}{4D^* t}\right], \tag{16}$$

where u is the averaged fluid velocity and D^* the dispersion coefficient. Therefore, the dimensionless time (defined by using L^2/D^* as characteristic time) at which the maximum concentration is recorded at the outlet can be easily calculated as

$$t_{\max} = \frac{(\sqrt{1+Pe^2} - 1)}{Pe^2}, \tag{17}$$

where $Pe = uL/D$ is the Peclet number.

The dispersion coefficient can be determined based on the approach of Salles et al. [48] and is found in this case to be $D^* = 1.34D$. Then, Eq. (17) gives $t_{\max} = 0.047$ for $Pe = 20$, when the numerically calculated value is 0.048, as shown in Fig. 3 where the outlet concentration is plotted versus time. Note that the dimensionless time step dt must be small enough ($< 10^{-5}$) to attain acceptable accuracy in the calculations.

4. Results and discussion

In a first step, we wish to recall the calculated flow fields in the sphere-in-cell model, resulting from Eqs. (2a) and (2b) (see Fig. 1b) as well as in a stochastically constructed spherical particle assemblage with porosity $\varepsilon = 0.7243$, resulting from the solution of the Stokes equations (13a) and (13b) (see Fig. 2b). This visualization of the respective flow fields allows for an appreciation of the differences between the two

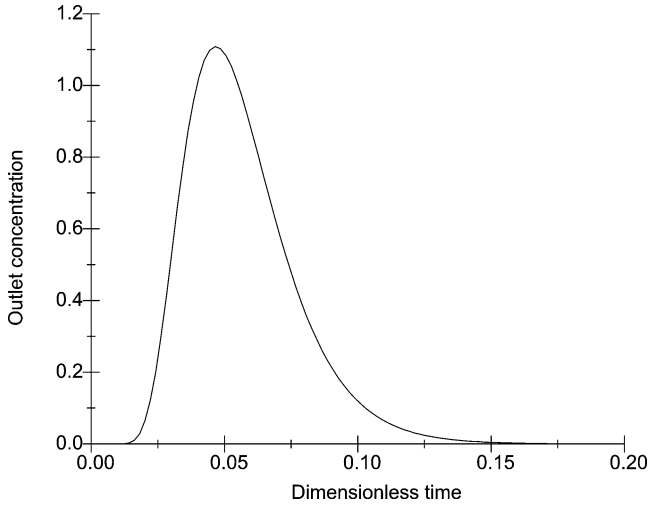

Fig. 3. Outlet concentration profile for $Pe = 20$ in a periodic array of spheres.

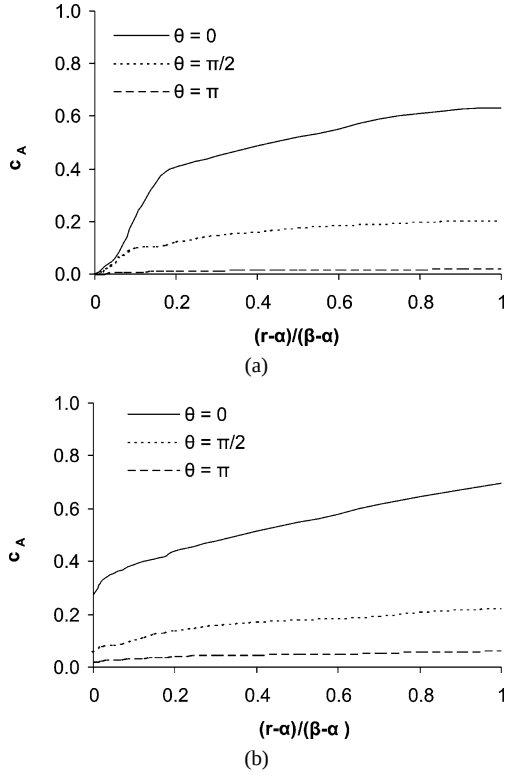

Fig. 4. Spatial concentration profiles for $Pe = 15$ and $\varepsilon = 0.9$ at three different angular positions of the sphere-in-cell for instantaneous (a) and Langmuir-type (b) adsorption.

velocity fields that are used as input for the solution of the mass transfer problem in these geometries.

Figure 4 shows the spatial concentration profiles for substance A at different angular positions in a high-porosity sphere-in-cell model ($\varepsilon = 0.9$) for the cases of instantaneous (a) and Langmuir-type (b) adsorption. The ratio k/K, appearing in Eq. (7), has been set to 1 and this value is used everywhere in this study unless otherwise stated. The Peclet value is low ($Pe = 15$); however, it has been selected to be high enough to ensure the satisfaction of the condition $\partial c_A/\partial r = 0$ at $r = \beta$ and $\theta = 0$. A gradual decrease of the concentration is observed for constant r as the angular position approaches the outlet because of the shape and extent of the concentration boundary layer (see Fig. 1b). Therefore, the possibility for substance A to be captured by the solid surface becomes lower with the angular position, although the accessibility of the solid surface is in general high due to the rather diffusive character of the flow (low Peclet). In general, higher concentration gradients at any radial and angular position are found for the case of instantaneous adsorption compared to those for Langmuir-type adsorption, as the surface concentration, $c_A(\alpha, \theta)$, is much higher in the second case, taking its higher value at the impact point and decreasing monotonically as θ tends to π.

The dependence of the adsorption efficiency on the Peclet number for instantaneous (a) and Langmuir-type (b) adsorption modes and for several porosities ($\varepsilon = 0.9883$, $\varepsilon = 0.8136$, and $\varepsilon = 0.7243$) is presented in Fig. 5 for the sphere-in-cell model. In general, higher efficiency is found for instantaneous adsorption compared to the Langmuir type, as the concentration gradients are lower in the latter case. Indeed, the concentration on the solid surface attains in the case of Langmuir type of adsorption non-zero values, rendering the overall driving force $c_A(\beta, \theta) - c_A(\alpha, \theta)$ smaller. It is also evident that as porosity decreases, higher efficiencies are found for both adsorption modes as the available adsorbing mass of solid increases. A sharp decline of the adsorption efficiency is observed at low *Pe* with a smoother decrease for *Pe* larger than about 20 in the case of Langmuir adsorption (for all porosities in Fig. 5b). This general trend of efficiency with *Pe* is expected, as the more convective flows (increasing Peclet) tend to prevent substance A from being captured by the solid surface. Interestingly, in Fig. 5a (instantaneous adsorption) this sharp decline behavior holds only for the very large porosity. It seems that the larger concentration gradients close to the solid surface in this case (compared to Langmuir adsorption) compensate partially for the convective character of the flow and the reduction of efficiency with increasing Peclet is considerably smoother in Fig. 5a for the smaller porosity values (in fact, one needs Peclet values larger than 50 to start obtaining efficiencies lower than unity for $\varepsilon < 0.9$ in Fig. 5a).

The discrete points in Fig. 5c represent the experimental data of Wilson and Geankoplis [49] for $\varepsilon = 0.7$ (the highest porosity used in their experiments). As these authors have in fact measured the overall Sherwood number, *Sh*, defined in the sphere-in-cell geometry as $Sh = \alpha k_0/D$, where k_0 is the overall mass transport coefficient, we had to transform it to adsorption efficiency, λ_0, to allow for comparison with the predictions. Starting from the definition of adsorption efficiency in Eq. (11), the numerator (r-component of the molar flux on the adsorbing surface) can be expressed through the use of the mass transfer coefficient as $k_0 \Delta C S_{\text{sphere}}$. This leads after some algebraic manipulations to the following

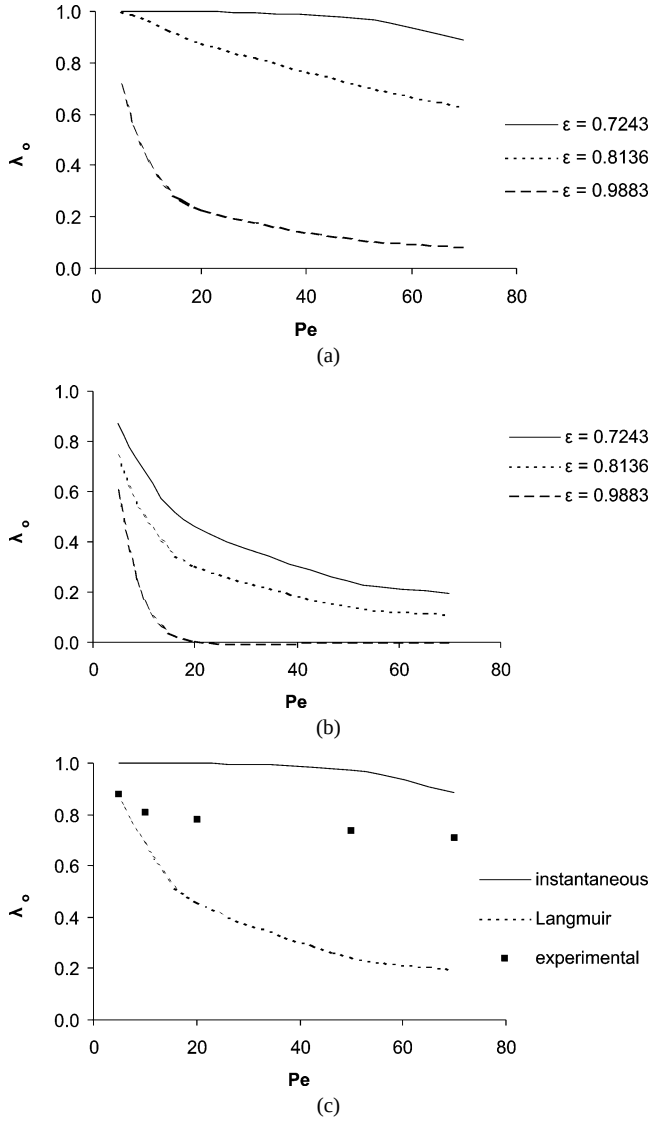

Fig. 5. Adsorption efficiency of the sphere-in-cell model as a function of *Pe* for various porosities: instantaneous (a) and Langmuir type (b) adsorption. In (c) the efficiencies calculated for instantaneous (solid line) and Langmuir-type (dashed line) adsorption (for $\varepsilon = 0.7243$) are compared to experimental data (discrete points [46]).

linear relation between the overall Sherwood number and λ_0,

$$Sh = \lambda_0 \frac{Pe}{(1-\varepsilon)} \frac{R}{L} \frac{c_{\text{in}}}{\langle c \rangle}, \tag{18}$$

where c_{in} is the inlet concentration and $\langle c \rangle$ is the known average concentration of substance A, respectively. Based on this, Fig. 5c compares the adsorption efficiencies calculated for instantaneous and Langmuir-type adsorption mechanisms in the sphere-in-cell with the above-mentioned experimental data. As the adsorption mechanism in the experiments is not clearly known, the agreement between predictions and experimental data can be considered as sufficient. In fact, one could vary the ratio k/K of Eq. (7) until a full match between computed and measured efficiencies is achieved. We do not pursue this exercise further here as there is no information on experimental k/K values.

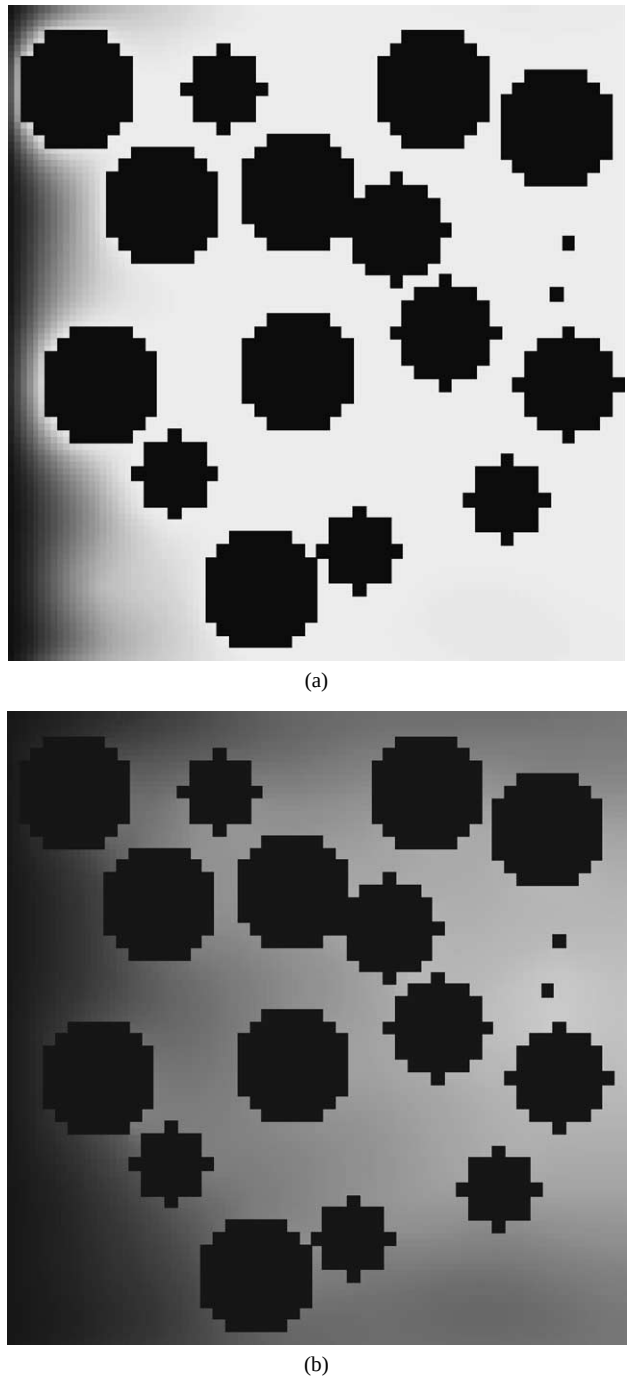

Fig. 6. Spatial distribution of the concentration of substance A within a 2-D cut of the 3-D sphere assemblage for instantaneous (a) and Langmuir-type (b) adsorption (flow inlet is on the left side of the images; darker areas correspond to higher concentrations).

Turning to the 3-D spherical particle assembly, the spatial distribution of the concentration, obtained numerically for $Pe = 20$ and $\varepsilon = 0.7243$ along the flow direction, is presented in Fig. 6 where a 2-D cut of the stochastically constructed medium is visualized for both instantaneous (a) and Langmuir-type (b) adsorption. The concentration is higher

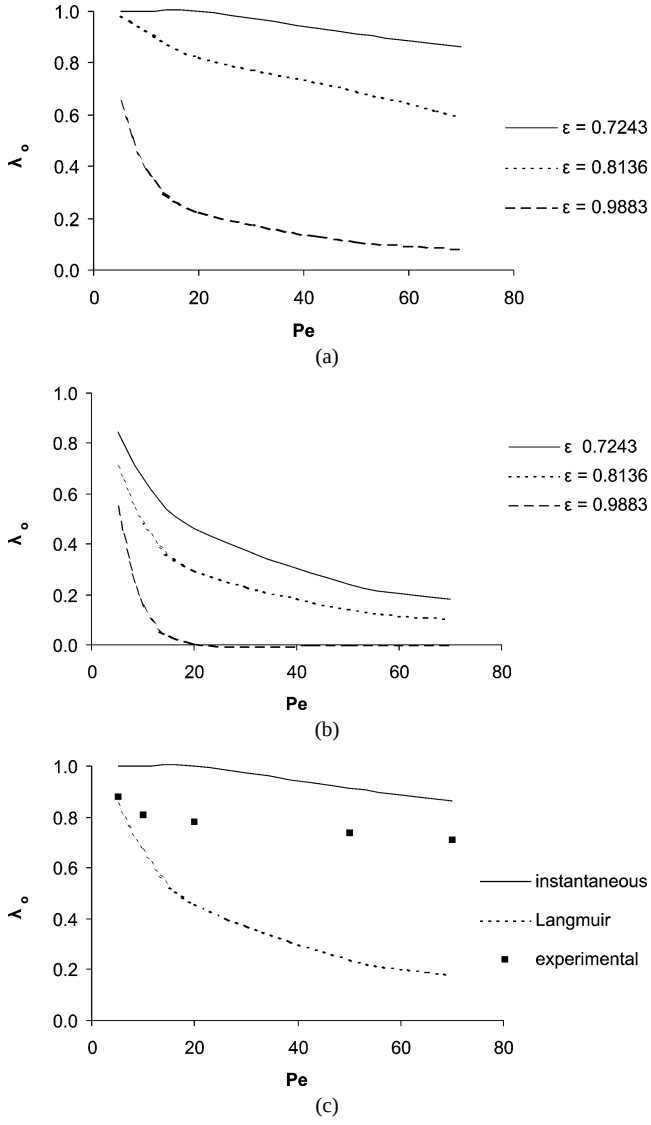

Fig. 7. Adsorption efficiency of the 3-D sphere assemblage as a function of *Pe* for various porosities: instantaneous (a) and Langmuir-type (b) adsorption. In (c) the efficiencies calculated for instantaneous (solid line) and Langmuir-type (dashed line) adsorption (for $\varepsilon = 0.7243$) are compared to experimental data (discrete points [46]).

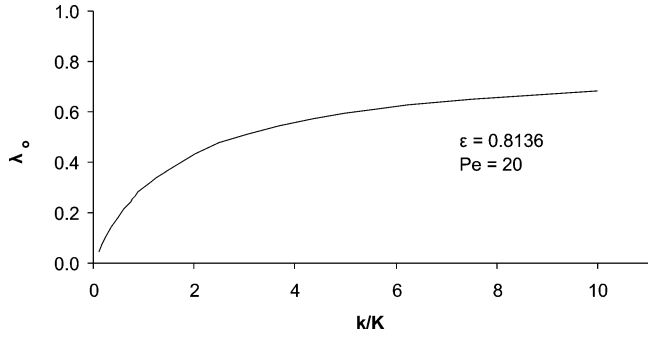

Fig. 8. The effect of the ratio k/K on the adsorption efficiency.

on the left side of the images (inlet) and gradually decreases along the medium in a manner that is significantly steeper for the instantaneous than for Langmuir-type adsorption. In addition, the adsorption efficiency for several porosities ($\varepsilon = 0.9883$, $\varepsilon = 0.8136$, and $\varepsilon = 0.7243$) and Peclet numbers is calculated by the full-numerical scheme in the sphere assembly for instantaneous (a) and Langmuir-type (b) adsorption and presented in Fig. 7. The effects of porosity and Peclet on the adsorption efficiency are the same as those mentioned above when discussing the sphere-in-cell results of Fig. 5 (higher efficiencies correspond to lower porosity while increasing Peclet numbers lead to lower λ_0 values). Moreover, the consideration of instantaneous adsorption leads to higher values of the adsorption efficiency at the same Peclet number and porosity than those calculated under the assumption of a Langmuir-type adsorption. Finally, it must be noted that similar agreement between predictions and experimental data is shown in Fig. 7c as in the sphere-in-cell case of Fig. 5c.

The influence of the ratio k/K, defined in Eq. (7), on the computed adsorption efficiency is presented in Fig. 8 for $Pe = 20$ and $\varepsilon = 0.8136$. As this ratio increases, a significant enhancement of λ_0 is observed because higher k/K corresponds to lower ratios of the covered surface, Θ_{eq}. This in turn corresponds to lower surface concentrations as it can be easily shown with the use of Eq. (10) and to higher concentration gradients, i.e., to higher λ_0. On the other hand, the increment of the ratio k/K can be viewed as a higher adsorption rate for a given K value and, thus, less mass of the substance A can escape from the solid surfaces; i.e., higher λ_0 values result.

It is interesting to consider the relative agreement between the results produced by considering the sphere-in-cell approximation and those obtained from the numerical solution in the 3-D sphere assemblages. Figure 9a compares the respective adsorption efficiencies for porosity approaching unity ($\varepsilon = 0.9883$) and instantaneous adsorption. It is obvious that the agreement is perfect as the semi-analytical sphere-in-cell model is very close to reality for such high-porosity values. When lower porosities are considered, the fundamental assumptions of the sphere-in-cell approximation are less and less satisfied [8,9]. Indeed, in the low *Pe* regime that is characterized by the gradual dominance of the diffusive over the convective terms, the semi-analytical approach of the sphere-in-cell model cannot adequately describe the mass transport process, as the diffusion layer is very thick (larger than the cell itself) and tends to infinity as $Pe \to 0$. On the other hand, as *Pe* increases, the flow becomes more and more convective and the analytical flow field of the sphere-in-cell is not any more a sufficient approximation of the actual flow field in real granular media, thus leading to discrepancies of the model. As shown in Figs. 9b and 9c, however, for $\varepsilon = 0.8136$ and $\varepsilon = 0.7243$ the agreement between the two approaches remains from very good to satisfactory in the range of *Pe* considered. This is somehow expected since both the sphere-in-cell and the sphere assemblage geometries used in the present study are constructed such that they are characterized by the same porosity and internal (adsorbing) surface area. This has been accomplished

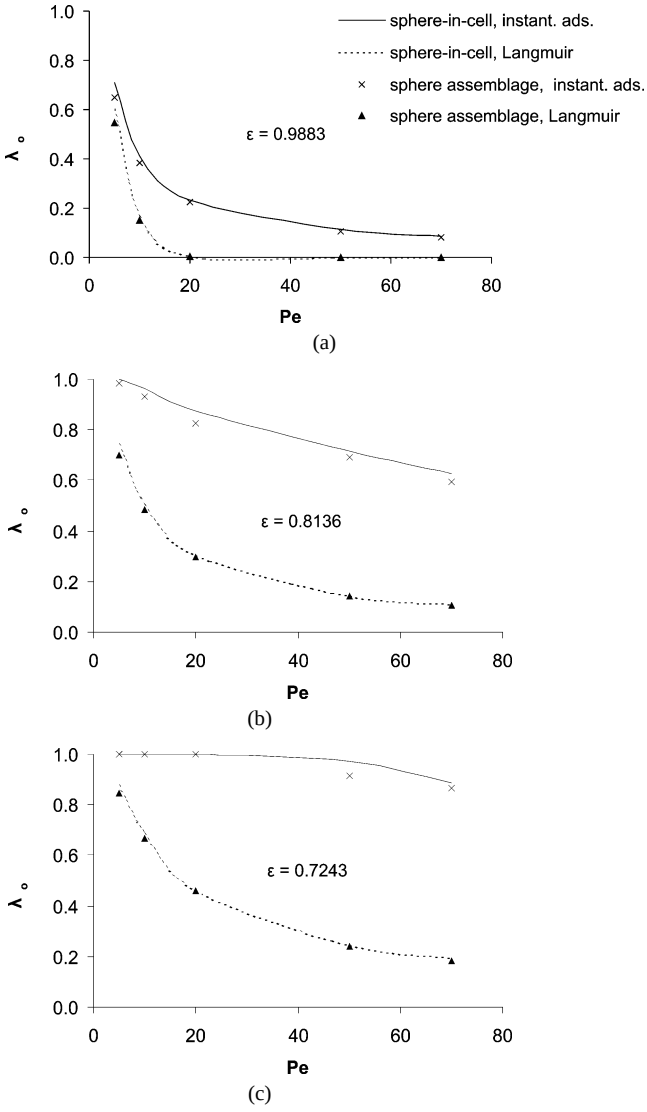

Fig. 9. Comparison between adsorption efficiency in sphere-in-cell and sphere assemblies for different porosities.

by selecting the proper radius and population number of spheres in the assemblage. Of course, it is possible to construct several sphere assemblages of the same porosity but with varying sphere radius and population number and therefore with different internal surfaces. Figure 10 shows how this affects the calculated adsorption efficiency for instantaneous and Langmuir adsorption. In the figure, the horizontal axis represents the internal surface ratio, which changes as different media are considered. The case of ratio equal to unity corresponds to the results discussed so far in this work. Evidently, λ_0 is not influenced significantly under instantaneous adsorption conditions by the change in the medium. This is again due to the high concentration gradients prevailing in this case and masking in essence the effect of the internal surface variation. However, in the more realistic Langmuir type of adsorption a very pronounced influence on λ_0 is observed, implying that caution should be exercised when using the sphere-in-cell model for the determination of

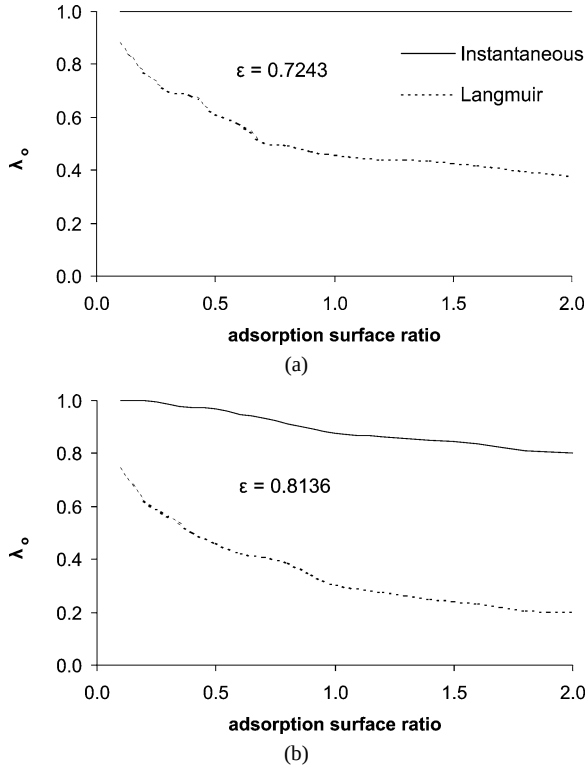

Fig. 10. The effect of using sphere assemblages with constant porosity and varying internal surface area on adsorption efficiency.

adsorption efficiency in granular media. Matching of porosity alone is not sufficient for a reliable result in that respect.

5. Conclusions

Analytical and numerical investigations for the mass transport from a moving Newtonian fluid to an assemblage of spherical solid absorbers are presented for $Pe < 10^2$ and relatively large porosities ($\varepsilon > 0.7$). At higher *Pe* the overall problem is amenable to analytical treatment with sufficient accuracy in the simplified geometry of the sphere-in-cell model as the flow field therein can be taken as a good enough approximation of the real one and certain diffusive terms can be safely neglected. In the present work, we focus on the low to moderate *Pe* regime where the sphere-in-cell approach permits the analytical determination of the velocity field, which is then used for the solution of the convection–diffusion equation within the domain defined by the cell. In addition, we attempt a numerical solution of the flow field and the corresponding convection–diffusion problem in the more realistic geometry of stochastically constructed 3-D sphere assemblages. In all cases, we consider (a) no adsorption, (b) instantaneous adsorption, and (c) Langmuir-type adsorption. The adsorption efficiency is calculated as a function of *Pe* and porosity and the adequacy of the simplified semi-analytical approach is tested against the predictions from the numerical study in sphere assemblages. It is found that higher adsorption efficiencies correspond to lower

porosity while increasing Peclet numbers lead to lower λ_0 values. Moreover, the consideration of instantaneous adsorption yields higher values of the adsorption efficiency at the same Peclet number and porosity than those calculated under the assumption of a Langmuir-type adsorption. Overall, the sphere-in-cell approach seems to be an adequate model for relatively high-porosity media and moderate to large Peclet values provided that a proper account of the actual porous media properties (porosity and internal surface area) is taken. A simple match of porosity is not sufficient for a reliable estimation of adsorption efficiencies. The validity of the simplified geometry is less pronounced for low *Pe* where diffusion is dominant.

References

[1] R.S. Rayleigh, Philos. Mag. 34 (1892) 481.
[2] R.E. Meredith, C.W. Tobias, J. Appl. Phys. 31 (1960) 1270.
[3] J.G. Berryman, Phys. Rev. A 27 (1983) 1053.
[4] P. Meakin, A.T. Skjeltrop, Adv. Phys. 42 (1993) 1.
[5] W.M. Visscher, M. Bolsterli, Nature 239 (1972) 504.
[6] R. Jullien, P. Meakin, Europhys. Lett. 4 (1987) 1385.
[7] D. Coelho, J.-F. Thovert, P.M. Adler, Phys. Rev. E 55 (1997) 1959.
[8] J. Happel, AIChE J. 4 (1958) 197.
[9] S. Kuwabara, J. Phys. Soc. Jpn. 14 (1959) 527.
[10] G.H. Neale, N. Epstein, W.K. Nader, Chem. Eng. Sci. 28 (1973) 1865.
[11] G.H. Neale, W.K. Nader, AIChE J. 19 (1973) 112.
[12] G.H. Neale, W.K. Nader, AIChE J. 20 (1974) 530.
[13] N. Epstein, J.H. Masliyah, Chem. Eng. J. 3 (1972) 169.
[14] D. Prasad, K.A. Narayan, R.P. Chhabra, Int. J. Eng. Sci. 28 (1990) 215.
[15] A.K. Jaiswal, T. Sundararajan, R.P. Chhabra, Int. J. Eng. Sci. 31 (1993) 293.
[16] R. Lemaitre, P.M. Adler, Transp. Porous Media 5 (1990) 325.
[17] A.N. Galani, et al., in: Proceedings of IMECE 2001, ASME Int. Mech. Eng. Congress & Exposition, New York, November 11–16, 2001.
[18] V.G. Levich, Physicochemical Hydrodynamics, Prentice–Hall, Englewood Cliffs, NJ, 1962.
[19] R. Pfeffer, J. Happel, AIChE J. 10 (1964) 605.
[20] R. Pfeffer, Ind. Eng. Chem. Fundam. 3 (1964) 380.
[21] K.K. Sirkar, Ind. Eng. Chem. Fundam. 14 (1975) 73.
[22] G.I. Tardos, C. Gutfinger, N. Abuaf, AIChE J. 22 (1976) 1147.
[23] M. Quintard, S. Whitaker, Adv. Water Res. 17 (1994) 221.
[24] S. Bekri, J.F. Thovert, P.M. Adler, Chem. Eng. Sci. 50 (1995) 2765.
[25] V.V. Mourzenko, S. Bekri, J.F. Thovert, et al., Chem. Eng. Commun. 150 (1996) 431.
[26] S. Bekri, J.F. Thovert, P.M. Adler, Eng. Geol. 48 (1997) 283.
[27] S.W. Churchill, Chem. Eng. Commun. 24 (1983) 339.
[28] M.M. El Kaissy, G.M. Homsy, Ind. Eng. Chem. Fundam. 12 (1973) 82.
[29] R. Clift, J.R. Grace, M.E. Weber, Bubbles, Drops and Particles, Academic Press, New York, 1978.
[30] L.A. Romero, SIAM J. Appl. Math. 54 (1994) 42.
[31] R.J. Han, O.R. Moss, B.A. Wong, J. Aerosol Sci. 27 (1996) 235.
[32] J.H. Masliyah, N. Epstein, Prog. Heat Mass Transfer 6 (1972) 613.
[33] V.N. Burganos, F.A. Coutelieris, A.C. Payatakes, AIChE J. 43 (1997) 844.
[34] C.Y. Wen, L.Y. Wei, AIChE J. 17 (1971) 272.
[35] H.B. Lu, N. Mazet, B. Spinner, Chem. Eng. Sci. 51 (1996) 3829.
[36] R. Wanker, H. Raupenstrauch, G. Staudinger, Chem. Eng. Sci. 55 (2000) 4709.
[37] F.A. Coutelieris, Stud. Surf. Sci. Catal. 144 (2002) 745.
[38] M.D. Mat, Y. Kaplan, Int. J. Hydrogen Energy 26 (2001) 957.
[39] J.B. Rosen, J. Chem. Phys. 20 (1952) 387.
[40] T.W. Weber, R.K. Chakravorti, AIChE J. 20 (1974) 228.
[41] K. Shams, Chem. Eng. Sci. 56 (2001) 5383.
[42] F.A. Coutelieris, V.N. Burganos, A.C. Payatakes, AIChE J. 41 (1995) 1122.
[43] P.M. Adler, C.J. Jacquin, J.A. Quiblier, Int. J. Multiphase Flow 16 (1990) 691.
[44] E.S. Kikkinides, V.N. Burganos, Phys. Rev. E 59 (1999) 7185.
[45] M.E. Kainourgiakis, E.S. Kikkinides, A.K. Stubos, J. Porous Mater. 9 (2002) 141.
[46] R.B. Bird, W.E. Stewart, E.N. Lightfoot, Transport Phenomena, Wiley, New York, 1960.
[47] M. Sahimi, Rev. Mod. Phys. 65 (1993) 1393.
[48] J. Salles, et al., Phys. Fluids A 5 (1993) 2348.
[49] E.J. Wilson, C.J. Geankoplis, Ind. Eng. Chem. Fundam. 5 (1966) 9.